Separation and Purification Technology 320 (2023) 124119

Contents lists available at ScienceDirect

Separation and Purification Technology

journal homepage: www.elsevier.com/locate/seppur

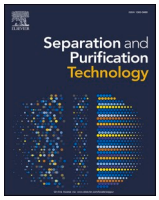

Degradation of organic pollutants combining plasma discharges generated within soil with TiO_2 and ZnO catalysts: Comparative analysis, optimization and mechanisms

M. Hatzisymeon [a,b], M.K. Daletou [c], G. Rassias [b], C.A. Aggelopoulos [a,*]

[a] Laboratory of Cold Plasma and Advanced Techniques for Improving Environmental Systems, Institute of Chemical Engineering Sciences, Foundation for Research and Technology Hellas (FORTH/ICE-HT), 26504 Patras, Greece
[b] Chemistry Department, University of Patras, 26504 Patras, Greece
[c] Laboratory of Advanced Materials and Electrochemical Energy Conversion Devices, Institute of Chemical Engineering Sciences, Foundation for Research and Technology Hellas (FORTH/ICE-HT), 26504 Patras, Greece

ARTICLE INFO

Keywords:
Plasma-catalysis
Dielectric barrier discharge
Cold plasma
Photocatalysts
Trifluralin degradation
Soil remediation

ABSTRACT

An advantageous plasma-catalytic setup was developed and applied towards the degradation of trifluralin in soil. For the first time, TiO_2 and ZnO catalysts were compared when employed in conjunction with micro-discharges generated directly into the interconnected soil channels. In the presence of catalysts, a significant increase in degradation efficiency was observed; after 5 min, trifluralin degradation increased from 66.5% (plasma alone) to 94.2% and 93% with the addition of TiO_2 and ZnO, respectively. In terms of degradation kinetics, TiO_2 was a slightly superior catalyst compared to ZnO whereas both catalysts performed better under oxygen than in air atmosphere. Compared to plasma alone, the plasma-catalytic treatment considerably increased (~3fold) the process energy efficiency. Moreover, the inhibitory effect of soil moisture was less pronounced during TiO_2 plasma-catalysis where a reduction of ~19% in pollutant degradation was observed at 5 wt% soil moisture compared to a ~54% reduction during plasma alone. The addition of TiO_2 and ZnO resulted in a significant increase in NO_2 concentration and a noticeable reduction in O_3 generation associated with an increase of certain plasma species concentration and the generation of additional and more active ROS, respectively. Liquid chromatography (UPLC/MS) data at the early stages of the trifluralin degradation revealed similar intermediates and degradation processes between plasma-alone and plasma-catalysis. The present effort supports the potential of future implementation of a plasma-catalytic soil remediation method being a rapid, highly efficient, low energy demanding and green method.

1. Introduction

Soil has long been proposed as the "most complex biomaterial on the planet". This is a reasonable claim considering that it acts as a habitat for living organisms, a hydrological regulator of water quality and quantity and a nutrient source tank. As a consequence of human activities, a myriad of organic pollutants including pesticides, pharmaceuticals, polycyclic aromatic hydrocarbons (PAHs) and flame retardants ends up in soil [1].

Several advanced oxidation processes have been applied to soil remediation, with plasma discharge being most attractive due to its efficient process with minimal time and secondary pollution. To date, cold atmospheric plasma (CAP) has been widely applied for water purification being an innovative, green and highly efficient method for the removal of organic pollutants; its superior performance is based on the high oxidation potential of the plasma-generated reactive oxygen and nitrogen species (RONS), such as hydroxyl radicals (•OH), singlet oxygen ($^1O_2$), atomic oxygen (•O), ozone (O_3) and nitrogen oxides (NO_x) [2]. However, during the last decade, more and more CAP efforts have been also applied for the remediation of polluted soil [2–5]. Remediation efficiency is strongly affected by various parameters (e.g. treatment time, plasma gas and flow rate, applied voltage), the chemistry of the pollutants, the properties of the soil and the plasma reactor configuration. Among the various plasma systems, dielectric barrier discharge (DBD) and pulsed corona discharge (PCD) are the most frequently used being effective against different types of contaminants including diesel

* Corresponding author.
E-mail address: caggelop@iceht.forth.gr (C.A. Aggelopoulos).

https://doi.org/10.1016/j.seppur.2023.124119
Received 13 March 2023; Received in revised form 3 May 2023; Accepted 15 May 2023
Available online 20 May 2023

fuel [6], non-aqueous phase liquids (NAPLs) [7,8], polyaromatic hydrocarbons (PAHs) [9,10], pesticides [11,12], antibiotics and perfluorooctanoic acid (PFOA) [13].

In all the aforementioned studies, plasma reactive species were generated above the contaminated medium and afterwards diffused from the gas phase into the soil void to reach the pollutants, raising concerns about efficient mass transport. Recently, the generation of plasma discharges directly inside the pore network of the contaminated soil revealed improved process energy efficiency due to the enhancement of the mass transport and interaction of plasma species with the pollutant molecules [14–16]. In addtion, when high voltage nanosecond pulses (NSP) were used to generate the plasma, an extremely high energy efficiency of the degradation process was achieved [16,17]. Given that plasma-catalysis is an emerging field with promising results in the field of wastewater treatment [2,18–20], a step forward in soil remediation could be the combination of the most energy efficient plasma reactor (i.e. HV nanopulses to generate RONS directly inside soil pores) with catalysts.

To the best of our knowledge, studies combining plasma with catalysts for soil remediation are scarce whereas plasma-catalytic mechanisms remain unexplored. The well-known photocatalyst titanium dioxide (TiO_2) was first explored combined with plasma, achieving ~14% higher degradation of p-nitrophenol [21,22]. Several parameters (catalyst loading, soil moisture and pH) were explored and degradation processes were proposed. More recently, the addition of TiO_2, as well as CeO_2 catalysts to a DBD system significantly improved the degradation of pyrene by 15–16% in both cases, highlighting the obvious synergistic effect with plasma [23]. In addition, the combination of a Ti-based metal organic framework catalyst with a DBD reactor resulted in increased degradation efficiency of fluorene in soil under relatively low applied voltage [24]. Apart from photocatalysts, the presence of Fe^0 was reported to accelerate the decomposition of chloramphenicol in DBD systems [25]. Finally, the combination of a pulsed discharge plasma system with Al_2O_3-supported metal oxide catalysts enhanced the removal efficiency of PAHs from soil, with MnO_2/γ-Al_2O_3 showing the best performance. Degradation efficiency increased up to 40%, although this required high catalyst loadings (23 wt%) [26].

It becomes apparent that non-thermal plasma in combination with catalysts can provide valuable pathways to efficient soil remediation. Titanium dioxide (TiO_2) and zinc oxide (ZnO) are two of the most widely used photocatalysts due to their low-cost, high surface area, robustness, abundance and non-toxicity [27–31]. Under the plasma discharge conditions, photocatalysts can be activated by ultraviolet radiation, as well as by the high energy electrons. Thus, ignition of plasma directly inside the soil matrix has the potential to strongly promote the penetration of radiation or species inside the entire volume of the soil to more effectively trigger the degradation reactions.

Hence, in this work, TiO_2 and ZnO catalysts were combined for the first time with plasma discharges generated directly inside the interconnected pore channels of the soil. Trifluralin was used as a model pollutant since it is one of the most common herbicides and classified by the World Health Organization (W.H.O) as neurotoxic, embryotoxic, carcinogenic and extremely toxic to aquatic organisms. Due to its hydrophobic nature, trifluralin has the potential to persist in soil for years depending on site-specific agro-climatic conditions [32]. The plasma-catalytic synergies were thoroughly studied, while the performance of the two catalysts was compared. Several experimental conditions in the presence/absence of catalysts were investigated, namely treatment time, catalyst loading, plasma gas and soil moisture. A detailed catalysts' characterization was performed, whereas the excited short-lived plasma species with and without catalysts in the gas phase along with the plasma-induced long-lived NO_2 and O_3 concentration in the reactor's exhaust gases were also determined. Furthermore, several plasma-induced oxidation intermediates of trifluralin were identified in soil providing insights into the mechanisms involved in the early stages of its degradation in the presence and absence of catalysts.

2. Experimental section

2.1. Materials and reagents

Trifluralin (PESTANAL, analytical standard) was provided by Sigma Aldrich and used as model pollutant. A clean sandy soil (purchased from Sigma Aldrich) was used as a model soil to investigate plasma-catalysis synergy without the interference of organic matter and microorganisms [33]. Soil porosity and moisture content were determined to be 0.49 and 0.1 wt%, respectively. The grain size distribution was in the range of 100–420 μm and its pH was equal to 7.5 when wet. TiO_2 (Titanium (IV) oxide nanopowder, 21 nm particle size P25, Sigma Aldrich), and ZnO (Zinc oxide nanopowder, <100 nm particle size, Sigma Aldrich) were used without any pretreatment. Methanol was of analytical grade (purchased from Sigma Aldrich) and used without further purification.

2.2. Catalysts morphology characterization before and after plasma

X-ray powder diffraction (pXRD) analysis took place employing a Bruker D8 Advance diffractometer with Cu Kα radiation ($\lambda = 1.5405$ Å) in the 2theta angle range 20 to 85°. Transmission electron microscopy (TEM) imaging was performed on a JEM2100 JEOL at 200 kV. SPECS Phoibos 100- 1D-DLD was employed for the X-ray photoelectron spectroscopy (XPS) under ultrahigh vacuum at room temperature using non-monochromatized Mg Ka radiation (20 eV analyzer pass energy). Charge correction took place for the spectra of all elements by fixing the binding energy of C 1 s at 284.6 eV. Mixed Gaussian-Lorentzian peaks with Shirley background were used for the analysis of the spectra.

2.3. Experimental setup, treatment conditions and electrical discharge properties

The schematic representation of the experimental setup used to treat contaminated soil samples and characterize the plasma is presented in Fig. 1a. The system consisted of a dielectric barrier discharge (DBD) reactor of coaxial geometry, a high voltage (HV) power supply (NPG-18/3500) able to produce positive nanosecond pulses (~4 ns), a gas supplying system, compartments for the electrical and optical characterization of the discharge, gas analyzers for the measurement of the plasma gaseous molecules (O_3 and NO_x) in the reactor exhaust gases and equipment for the chemical analysis of the plasma-treated soil samples.

The coaxial DBD reactor is presented in detail in our previous studies [15,16]. Briefly, the reactor consisted of a stainless-steel cylindrical HV electrode, a quartz dielectric tube and a stainless-steel grid attached to the exterior surface of the dielectric tube serving as the grounded electrode of the discharge. The soil was loaded and entirely filled the space between the HV electrode and the dielectric ensuring that micro-discharges were directly generated around the surface of the interconnected soil grains. Therefore, the novelty of this reactor lies on the production of micro-discharges within the contaminated soil allowing at the same time the simulation in the lab of an in-situ soil remediation by plasma (in-soil approach). Considering that this reactor configuration exhibited superior performance compared to plasma reactors where the plasma is produced above the soil surface [15,16], this is the first attempt to use this plasma system in conjunction with catalysts (Fig. 1b). The mass of the treated soil was 10.1 g, the HV electrode diameter was 18 mm, the electrode gap was 6.0 mm, the dielectric thickness was 1.7 mm whereas the soil thickness and length were 4.3 mm and 2.5 cm, respectively. Based on previous findings [16], the experiments were performed at constant flow rate (0.075 L min^{-1}) of various plasma working gases (air, oxygen and nitrogen) controlled by an Aalborg GFC17 mass flow controller. The pulse voltage was set equal to 22.2 kV and the pulse repetition rate was kept at 100 Hz.

A digital oscilloscope (Rigol MSO2302A, 300 MHz, 2 GSamples/s) was used for the electrical measurements by monitoring the waveforms of the current and the voltage nanopulses by means of a wideband

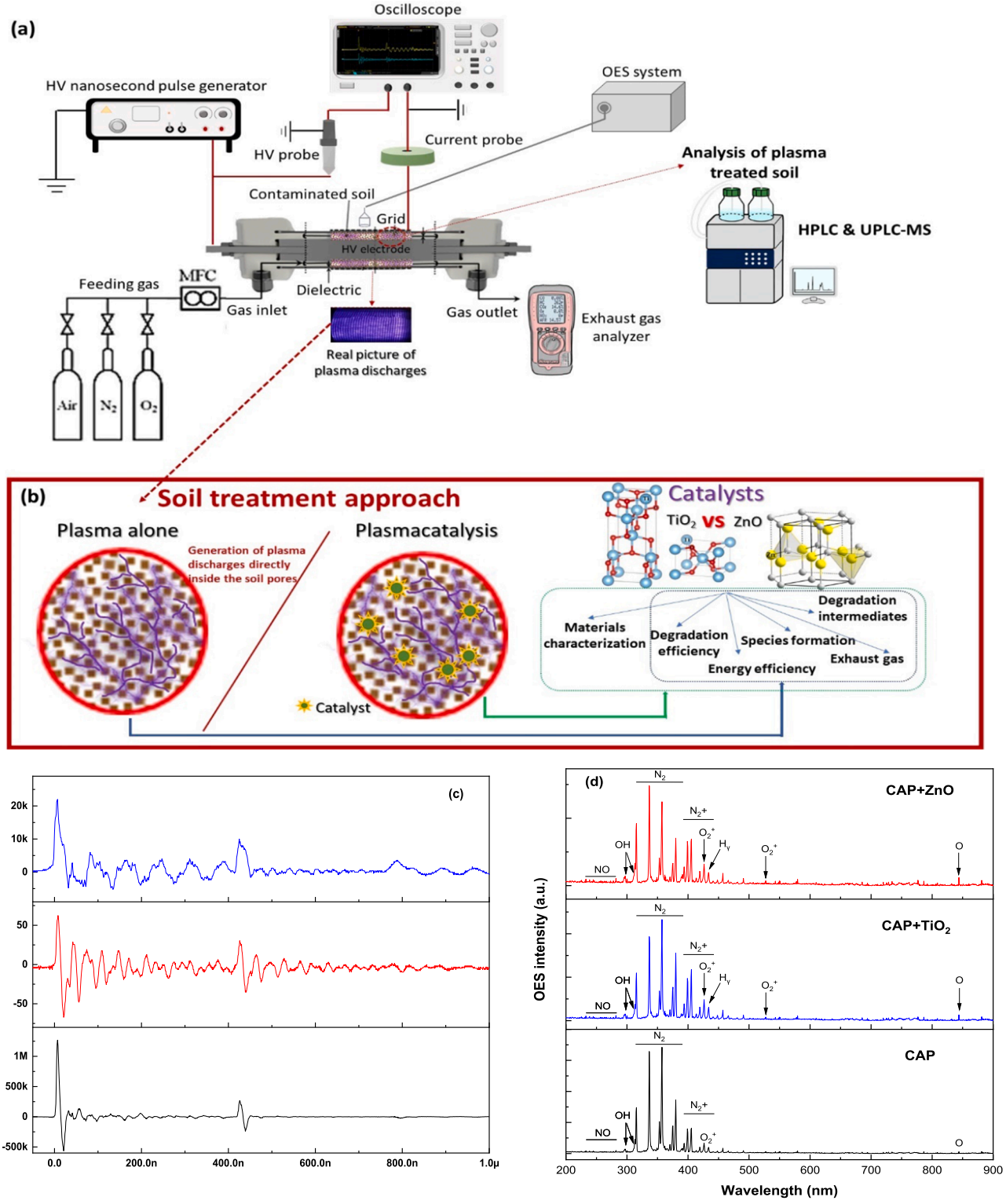

Fig. 1. (a) Schematic representation of the setup used to treat trifluralin-contaminated soil and characterize the plasma, (b) the main features of the soil treatment approaches followed in this study, (c) instantaneous voltage, current and power waveforms of the coaxial DBD reactor and (d) principal excited plasma species during plasma in the absence and in the presence of TiO_2 and ZnO (plasma gas: air, catalyst loading: 2 wt%).

current transformer (Pearson electronics 2877, 300 Hz-200 MHz) and a voltage probe (Tektronix P6015A, 0–75 MHz), respectively. The power (P) dissipated in the reactor, obtained as the average of five successive measurements, was determined by the following equation:

$$P = fE_p = f\int_{pulse} P(t)dt = f\int_{pulse} V(t)I(t)dt \quad (1)$$

where f is the pulse repetition rate, E_p is the pulse energy, while $P(t)$, $V(t)$ and $I(t)$ are the instantaneous power, voltage and current waveforms, respectively. The instantaneous voltage, current and power

waveforms are presented in Fig. 1c. The maximum pulse current was ~60 A which is ~2–3 orders of magnitude higher of the corresponding one measured in sinusoidal-driven DBD reactors (AC-DBDs) [12] leading to an enormously high instantaneous power ~1.3 MW (Fig. 1c). The very high instantaneous power along with the quite low mean DBD is the key of the extremely high energy efficiency of the nanosecond pulsed systems [34]. In particular, the mean DBD power was calculated equal to 0.46 (plasma alone) and 0.49 and 0.50 W for plasma+ZnO and plasma+TiO_2, respectively (Table S1), indicating no significant variation in DBD power between the various systems.

2.4. Detection of plasma species and measurement of temperature

Optical emission spectroscopy measurements were conducted for the identification of the main excited plasma species in the gas phase (Fig. 1d). Emission spectra of the plasma discharge in the range of 200–900 nm were recorded by means of a fiber optics spectrometer (AvaSpec-ULS2048CL-EVO, Avantes). The concentration of the plasma-generated NO_x and O_3 in the exhaust gases were recorded using a gas (Optima 7) and an ozone analyzer (Ozone Analyzer BMT 965, MES-STECHNIK), respectively. All aforementioned measurements were conducted in non-polluted soil in the presence and in the absence of catalysts; this could provide an important indication of the impact of the catalysts in the plasma process. A thermocouple attached to the ground electrode was used to measure the temperature via a digital multimeter (Mastech MS8209). The initial temperature was ~20 °C and increased slightly to ~22 °C at the end of the treatment (i.e. 10 min).

2.5. Preparation of contaminated soil, extraction and chemical analysis

The procedure followed for the contamination of soil samples included the dissolution of the pollutant in methanol under stirring and the subsequent immersion of the soil into the pollutant's solution. Afterwards, methanol was evaporated in a rotary evaporator at 50 °C, resulting in a homogeneously polluted soil with the initial concentration of trifluralin being 200 mg/kg-soil. Appropriate amounts of powdered TiO_2 and ZnO were fully mixed with the soil before the plasma-catalytic experiments resulting in various catalyst loadings in soil (i.e. 0.5, 1 and 2 wt%).

The recovery of organic compounds from soil samples was achieved using methanol as the extraction solvent. The extraction method is fully described in our previous work [15]. High-performance liquid chromatography (HPLC, Agilent 1100) coupled with a UV–Vis detector was used to quantify the residual concentration of trifluralin in soil. In order to identify relevant intermediates and compare their abundancies in the TiO_2 and ZnO plasma-catalytic processes against those manifested in the plasma alone conditions, samples taken after 1 min of treatment in each case were analyzed by UPLC/MS (details can be found in S2). The structure of the intermediates detected are proposed based on their molecular ions in positive and negative ionizations modes, fragmentation patterns and elution time (polarity) in the UPLC reverse phase column.

The determination of the pollutant degradation efficiency, $D(\%)$, was based on the following equation:

$$D(\%) = \left[\frac{C_0 - C}{C_0}\right] \times 100 \quad (2)$$

where C_0 and C are the trifluralin's concentration before and after plasma treatment, respectively. Statistically significant differences were evaluated using the analysis of variance Mann-Whitney test and were considered statistically significant at the level of at least $p \leq 0.05$.

In order to evaluate the degradation rate, a pseudo-first order reaction with respect to the pollutant concentration was assumed and the degradation kinetics were fitted using the following equation:

$$ln\left(\frac{C_0}{C}\right) = kt \quad (3)$$

where k is the apparent rate constant.

The calculation of the energy efficiency (E; mg/kJ) was done by the following equation:

$$E = \frac{m_{triflu}}{P \times t} \quad (4)$$

where m_{triflu} is the mass of the degraded trifluralin, t is the treatment time and P is the power of the DBD. All experiments were performed at least in triplicate exhibiting high reproducibility.

3. Results and discussion

3.1. The impact of plasma treatment on the catalysts' morphology

The catalysts were characterized prior to use with respect to their structure and morphology. Fig. S1 shows representative TEM images of the TiO_2 and ZnO samples, while the obtained XRD spectra are presented in Fig. S2. The almost spherical TiO_2 nanoparticles have a mean diameter close to 20 nm (Fig. S1), while the dominant phase (~90%) was anatase (Fig. S2). ZnO particles had a hexagonal wurtzite structure with a mean size <100 nm, within specifications. The surface area of ZnO is thus lower compared to that of TiO_2. Details regarding XRD analysis can be found in S3.

It is well reported that catalysts affect the plasma properties and vice versa. XPS measurements took place in order to study the surface chemical composition of the nanoparticles, as well as the oxidation state of the elements. In addition, the pristine samples were treated under air-plasma for 2 and 10 min to detect possible changes in the structure. Starting with the TiO_2 samples, upon the plasma treatment, the atom ratio O/Ti increased only slightly from 2.5 to 2.7 (Table S3a). Fig. 2a shows the Ti 2p XPS spectra of the different TiO_2 samples, where the standard Ti 2p3/2 and Ti 2p1/2 peaks can be seen. Ti^{4+} is the main valence state presenting a binding energy (BE) of the stronger Ti 2p3/2 at 458.5 eV (full width at half maximum FWHM = 1.4 eV) and a spin orbit splitting of 5.72 eV, according to literature [35,36]. The FWHM of Ti 2p3/2 was about 1.4 eV, as determined from the fitting. The 3^+ charge state would appear at about 1.8 eV lower than Ti^{4+} but the analysis of the spectra did not present such a component in any of the samples. As is evident from the figure, in the pristine sample, as well as after the plasma treatment, there was no observed peak shifting or any shoulder that could denote the presence of Ti^{3+} or any other oxides with intermediate Ti state. In this respect, plasma treatment followed in this work provoked no changes in the state of Ti element, unlike thermal plasma that has been reported to induce notable Ti-O bonds scission and oxygen deficiencies [37] evidenced also by a structural change and corresponding increase in the percentage of Ti^{3+} species.

Nevertheless, a small oxygen deficiency within the matrix is still possible thus, the oxygen core level spectra were measured and analyzed. Fig. 2b shows the XPS O 1 s spectra of the TiO_2 samples. A distinct increase of the peak's shoulder in the 531–533 eV region can be detected. Following this observation, all O 1 s spectra were deconvoluted as presented in the inset of the figure and the results are presented in Table S3a. More specifically, the main O 1 s peak is positioned at BE 529.8 eV and is attributed to the O-Ti lattice bond in TiO_2 [38]. The peak at 531.0 eV corresponds to a component related to oxygen vacancies [39] and seems to be slightly affected by the plasma treatment, while a serious increase in the peak at 533.3–533.5 eV was observed with increasing the plasma treatment time [40]. The latter peak (low binding energy component, LBEC) is commonly attributed to non-lattice oxygen which is associated with adsorption of the hydroxyl groups (Ti-OH) on the surface of amorphous TiO_2 [41]. Despite Ti and oxygen, a very small amount of nitrogen was also evidenced by XPS, in the pristine as well as

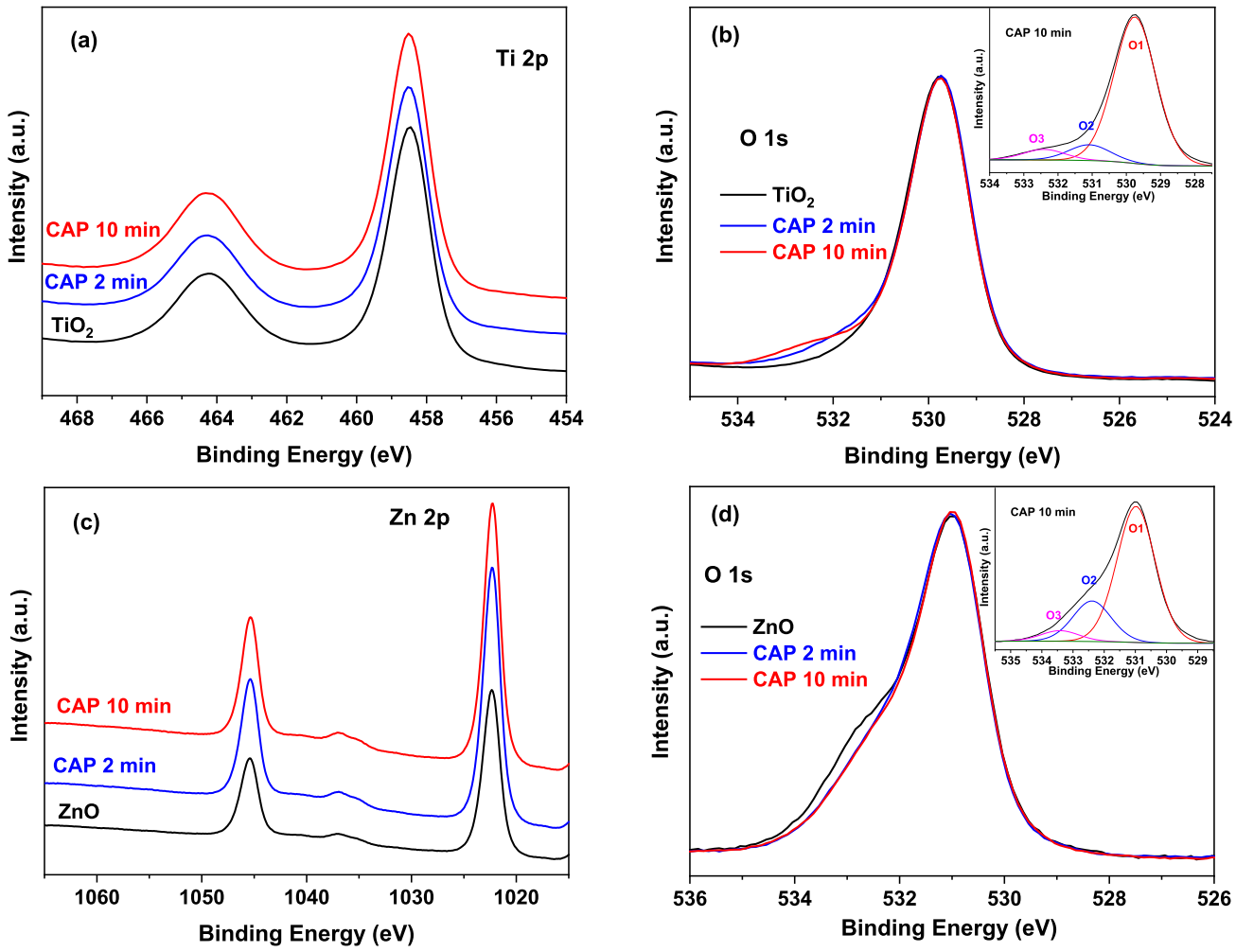

Fig. 2. XPS (a) Ti 2p, (b) O 1 s spectra of pristine TiO_2 and after 2 and 10 min of plasma treatment, (c) Zn 2p, (d) O 1 s spectra of pristine ZnO and after 2 and 10 min of plasma treatment. Insets in (b and d) show an example (for the sample after 10 min of plasma treatment) of the deconvolution of the oxygen spectra into single components (plasma gas: air).

the treated samples, that remained unaffected and positioned at about 400.3 eV (atom ratio N/Ti ~ 0.04), often in literature attributed to Ti-O-N species [42].

Fig. 2c shows the XPS Zn 2p spectra of ZnO, before and after plasma treatment. The characteristic Zn 2p doublet peaks appeared, corresponding to 2p3/2 and 2p1/2 having 23 eV difference between the two bonding energies, as is well reported for the 2^+ oxidation state of Zn [43–45]. The Zn 2p3/2 component is positioned at 1022.32–1022.37 eV [46] and the spectrum of the initial ZnO sample seems unaffected by the plasma treatment. According to the XPS spectra collected, the atom O/Zn ratio increased by 45–48% after plasma. The corresponding XPS O 1 s spectra are presented in Fig. 2d. Their direct comparison showed a change in the 532–534 eV region. The asymmetric peaks indicated the co-existence of different species thus the spectra were deconvoluted using three single components [47] O1 to O3 (FWHM about 1.44), Fig. 2d (inset) and Table S3b. The first peak O1 at about 531 eV is attributed to the oxygen atoms in a fully oxidized stoichiometric surrounding, in the Zn-O bonding of the ZnO wurtzite structure [46], while O2 peak is related to the oxygen deficiency or vacancies [44,48]. The final O3 peak at the highest BE is associated to weaker bonds of oxygen like OH group absorbed onto the surface [43]. The increased O/Zn ratio is accompanied by decreased percentage of the O2 and O3 oxygen components (Table S3b), which is in accordance with previous studies which showed that plasma treatment led to reduced oxygen vacancies and improved crystallinity [49,50]. In conclusion, the plasma treatment only enriched the surface of TiO_2 with non-lattice oxygen, whereas in the case of ZnO it affected the structure by seriously increasing the surface oxygen (increased O/Zn ratio). In the latter case, both the lattice oxygen (O1) and the vacancies (O2) increased after plasma, while their relative ratio (O2/O1) decreased.

3.2. *Effect of catalyst loading on degradation efficiency, rate and energy efficiency*

In order to determine the effect of both TiO_2 and ZnO catalysts on the trifluralin degradation efficiency, three different catalyst loadings in soil were investigated (Fig. 3). Each catalyst was homogenously mixed with soil at 0.5, 1 and 2 wt% loadings. The effect of different TiO_2 amounts on pollutant degradation is presented in Fig. 3a. Obviously, the presence of TiO_2 increased the degradation performance substantially in agreement with previously reported results on p-nitrophenol and pyrene degradation in soil by TiO_2-plasmacatalysis [22,23]. In particular, the increase of TiO_2 loading up to 1% increased the trifluralin degradation efficiency, especially at short treatment times, while higher TiO_2 loading (2 wt%), had a positive impact only on the pollutant degradation rate. For instance, after 2 min of plasma treatment, degradation efficiency was 30.9% for plasma alone process, while it increased to 44.8, 70.0 and 82.2% with the addition of 0.5, 1 and 2 wt% TiO_2, respectively. This positive TiO_2-effect was also reflected at higher treatment times; after 5 min the degradation efficiency increased from ~66.5% (CAP) to

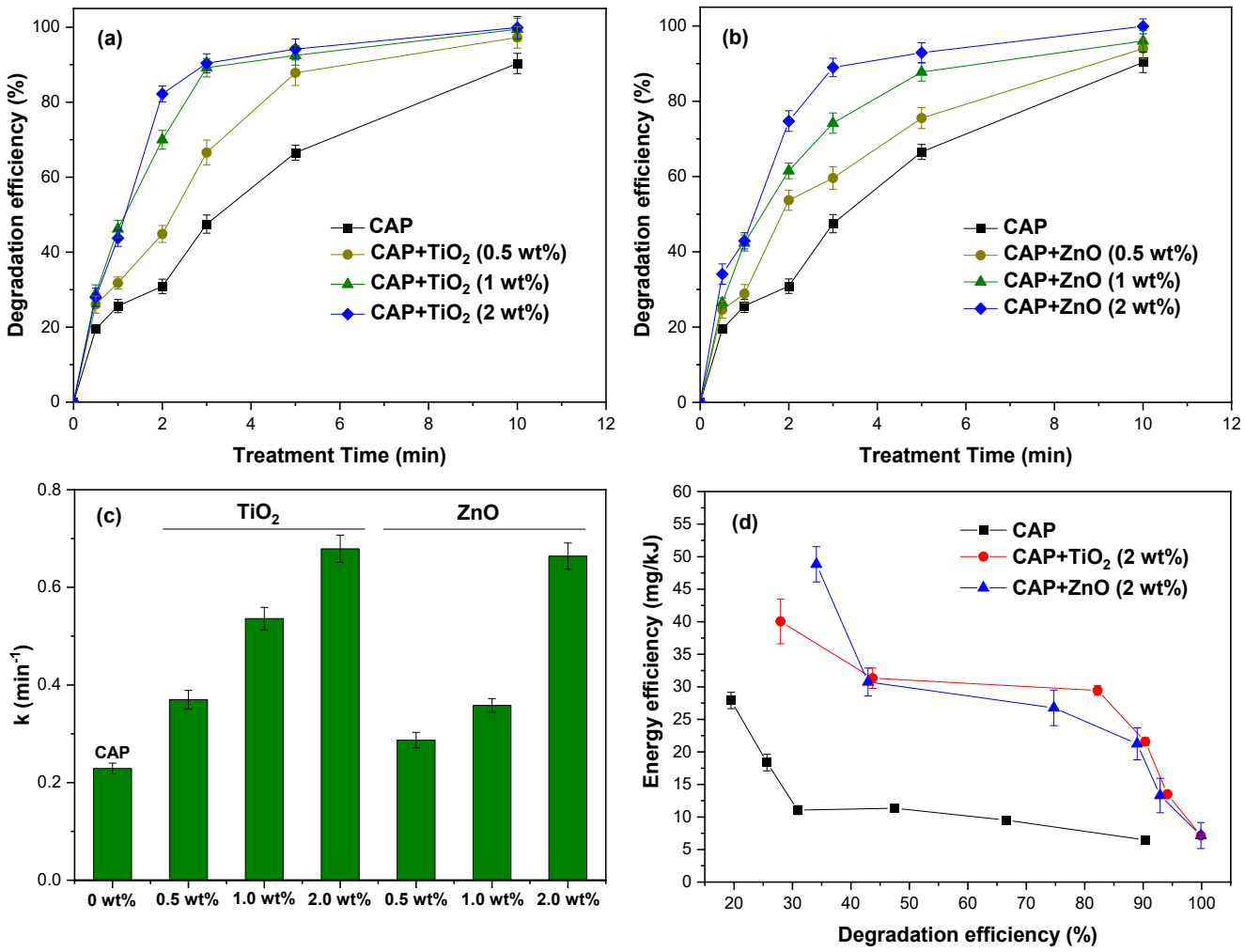

Fig. 3. Effect of (a) TiO_2 and (b) ZnO loading on trifluralin's degradation efficiency (plasma gas: air). (c) The pseudo-first-order apparent rate constants at different catalyst loading for both TiO_2 and ZnO and (d) the calculated energy efficiency (mg/kJ) of trifluralin's degradation in the presence and absence of TiO_2 and ZnO (plasma gas: air, catalyst loading: 2 wt%).

~94.2% at 2 wt% TiO_2 loading in soil. It is also noticeable that at the end of plasma treatment (10 min), the degradation of trifluralin was almost complete (>99.5%) in the presence of 1–2 wt% TiO_2 in contrast to plasma alone where trifluralin was degraded ~90% (Fig. 3a). The addition of ZnO catalyst also led to enhanced degradation of trifluralin (Fig. 3b). Indicatively, at short treatment times (i.e. 3 min), degradation efficiency was 47.5% for plasma alone, whereas it increased at 59.6, 74.2 and 89% with the addition of 0.5, 1 and 2 wt% ZnO, respectively. Similar to the TiO_2 effect, complete trifluralin's degradation was achieved (~99.9%) after 10 min of plasma+ZnO treatment.

The corresponding pseudo-first-order kinetics of trifluralin degradation at different catalyst loadings for both TiO_2 and ZnO are shown in Fig. S3. For both catalysts, the apparent rate constant k was an increasing function of catalyst loading (Fig. 3c). In particular, k increased from 0.23 min^{-1} (CAP) to 0.37, 0.54 and 0.68 min^{-1} at 0.5, 1 and 2 wt% TiO_2, respectively. Similarly, k increased to 0.29, 0.36 and 0.67 min^{-1} at 0.5, 1 and 2 wt% ZnO, respectively. It is noteworthy that a relatively higher catalytic activity was observed for TiO_2 at 0.5–1 wt% loading range, whereas at 2 wt% catalyst loading both catalysts performed equally (Fig. 3c). This may be rationalized by the vital role of plasma species in the degradation process and their relative concentration, which in turn depends on the type and loading of a catalyst (up to 1 wt%), while the equal catalytic activity of TiO_2 and of ZnO at a higher loading (2 wt%) is related to the similar concentrations of plasma species (e.g. NO_x, O_3) between the two catalysts (see results in section 3.5).

Because of the enhanced pollutant degradation, plasma-catalysis has been indicated as a valuable tool for enhancing process energy efficiency [2,21]. Various approaches have been adopted to increase the energy efficiency of plasma process including the use of HV nanosecond pulses (NSP) instead of sinusoidal high voltage and/or the generation of plasma discharges directly inside the soil pores in contrast to plasma creation above the contaminated medium [15,16]. In this respect, we calculated the energy efficiency (mg/kJ) of trifluralin's degradation in the presence and absence of TiO_2 and ZnO and the results are shown in Fig. 3d. Obviously, the presence of TiO_2 and ZnO significantly improved the energy efficiency of the system. It is worth noting that for ~90% trifluralin degradation, the calculated energy efficiency increased from 6.5 mg/kJ (CAP) to 21.6 mg/kJ (CAP+TiO_2) and 21.2 mg/kJ (CAP+ZnO) (Fig. 6d); that is a 330% improvement. After 5 and 10 min of treatment, where pollutant degradation was almost complete in the presence of TiO_2 and ZnO catalysts (~94 and >99.9%, respectively), the corresponding energy efficiencies were extremely high and equal to 13.5 mg/kJ and 7.2 mg/kJ.

Various cold plasma systems, including dielectric barrier discharge (DBD), pulsed corona and gliding arc, have been proposed for the degradation of organic pollutants in soil. Obviously, the energy efficiency of the current in-soil plasma-catalytic system driven by HV

Table 1
Degradation and energy efficiency of various plasma methods either in the presence or absence of catalysts for soil remediation.

CAP method	Catalyst/ Loading	Soil/ Pollutant	Degradation efficiency/ Treatment time	Energy efficiency (mg/kJ)	Ref
Nanopulsed-DBD in-soil discharges	–	Model sandy soil/Trifluralin (200 ppm)	90.3% (10 min)	6.5	This study
Nanopulsed-DBD in-soil discharges	TiO_2/2 wt%	Model sandy soil/Trifluralin (200 ppm)	90.4% (3 min) (i) >99.9% (10 min) (ii)	21.6 (i) 7.2 (ii)	This study
Nanopulsed-DBD in-soil discharges	ZnO/2 wt%	Model sandy soil/Trifluralin (200 ppm)	89% (3 min) (i) >99.9% (10 min) (ii)	21.2 (i) 7.2 (ii)	This study
AC-DBD ex-situ soil	–	Loamy soil/Pyrene (105 ppm)	79.7% (30 min)	0.0082	[10]
AC-DBD ex-situ soil	–	Model sandy soil/Atrazine (200 ppm)	84.6% (60 min)	0.3	[12]
Pulsed Corona ex-situ soil	–	Natural soil/PFOA (30 ppm)	71% (120 min)	0.0039	[13]
Pulsed Corona ex-situ soil	–	Natural soil/Phenanthrene (50 ppm)	74% (40 min)	0.1	[51]
Pulsed Corona ex-situ soil	No catalyst TiO_2/2 wt%	Natural soil/p-nitrophenol (800 ppm)	78.1% 88.8%	–	[22]
AC-DBD	No catalyst MOFs/0.1 wt%	Model sandy soil/Fluorene (100 ppm)	71.4% (10 min) 96.5% (10 min)	–	[24]
AC-DBD Parallel tubes	No catalyst TiO_2/CeO_2/-	Simulated soil/Pyrene (100 ppm)	25.5% (1 min) 66.2%/55.0% (1 min)	0.22 0.54/0.47	[23]

nanopulses is about 2–3 orders of magnitude higher compared to plasma systems driven by other HV power sources (e.g. AC, microsecond pulses) where plasma is produced above the soil surface (Table 1). The energy efficiency enhancement is related to the extremely high nanosecond instantaneous power (~1.3 MW, see Fig. 1c) in parallel to the very low mean power dissipated in the DBD (Table S1). Nevertheless, the addition of catalysts in our system increased further the energy efficiency (~3 fold) at a given value of pollutant degradation (Table 1, Fig. 3d). Complete pollutant degradation along with improved degradation kinetics and enormously high energy efficiency, suggests that the present nanopulsed in-soil plasma-catalytic reactor can be considered as the most energy efficient plasma system to date in the literature.

A comparison of energy efficiencies across the various remediation methods could better reveal the economic advantage of the present system. However, given that soil remediation is a multi-parameter process, only a rough estimation can be extracted. In this respect, a comparison of the energy efficiency between traditional soil remediation methods and the current plasma/plasma-catalytic systems is given in Table S4. Apparently, plasma-catalysis driven by HV nanopulses could be considered much more cost-effective compared to other methods. In particular, the current nanopulsed-DBD reactor where plasma discharges are created directly into the soil matrix could successfully remediate ~130 kg of soil/kWh, while its combination with TiO_2 or ZnO further improved the energy efficiency to ~410 kg of soil/kWh (based on the energy requirements for >90% remediation of 10.1 g of soil for each case).

Nevertheless, a drawback of plasma-catalysis is that it causes secondary pollution and therefore a non-dispersed method (e.g. catalyst immobilization) is required when applying catalysts to soil. The possibility of their easy separation from the soil at the end of the process can be considered through the use of catalysts or supports that exhibit magnetic separation capability such as Fe_3O_4, Fe_2O_3 and Co_3O_4 based composites. Very recently, the magnetic separable graphene-TiO_2-Fe_3O_4 nanocomposite was investigated for the plasma-catalytic removal of antibiotic oxytetracycline from water [52]. In addition, based on existing literature, TiO_2 and ZnO-based catalysts used in plasma-catalytic experiments for water treatment retained their activity, up to 97% in most cases, even after four or five cycles of use [53,54] which is promising for the sustainability of the present approach.

3.3. Effect of plasma gas on degradation efficiency in the absence and presence of catalysts

Plasma carrier gas controls the concentration and type of plasma-generated species thus strongly affecting the pollutant remediation efficiency [2,4]. In order to investigate the role of different RONS in trifluralin degradation, plasma and plasma-catalytic experiments were repeated under air, oxygen and nitrogen atmospheres. In the absence of catalysts, the results are shown in Fig. 4a. After 10 min of plasma treatment, degradation efficiency reached 90.3%, 91.7% and 23.9%, under air, O_2 and N_2 gases, respectively. Trifluralin degradation fitted a pseudo-first-order kinetic model (Fig. S4) with the apparent rate constant k being 0.23 (air-CAP), 0.24 (O_2-CAP) and 0.04 min^{-1} (N_2-CAP) (Fig. 4c). The similar degradation efficiency and rate under oxygen and air is in agreement with previous study on gasoline degradation in soil by pulsed corona [55]. The dominance of O_2-plasma and air-plasma towards trifluralin degradation could be attributed to the predominant role of plasma-generated ROS in comparison to RNS, given that an increased production of ROS is expected under oxygen-containing atmospheres compared to N_2 atmosphere. During O_2-plasma and air-plasma, electrons and various ROS (e.g. atomic oxygen, ozone, hydroxyl radicals) are generated through the reactions (5)-(7) contributing to the degradation of trifluralin:

$$e^- + O_2 \rightarrow 2{}^{\bullet}O + e^- \quad (5)$$

$$O_2 + {}^{\bullet}O \rightarrow O_3 \quad (6)$$

$$O + H_2O \rightarrow 2{}^{\bullet}OH \quad (7)$$

Since the O_2 content under O_2-plasma is higher compared to air-plasma and leads to higher ROS concentrations (e.g. O_3, see results below in section 3.5, Fig. 6), an increased degradation efficiency was expected under O_2-plasma. The essentially identical pollutant degradation in both cases indicated that even in the case of air-plasma, high ROS concentrations were provided reaching the limit where further increase did not seriously affect the reaction rate for the same pollutant concentration. However, it is also possible that NO_x generated from N_2 in the air (reactions 8–10) may contribute in the degradation process thus compensating for the reduction of ROS concentration in air-plasma compared to O_2-plasma.

$$N + O_2 \rightarrow NO + {}^{\bullet}O \quad (8)$$

$$N + 2{}^{\bullet}O \rightarrow NO_2 \quad (9)$$

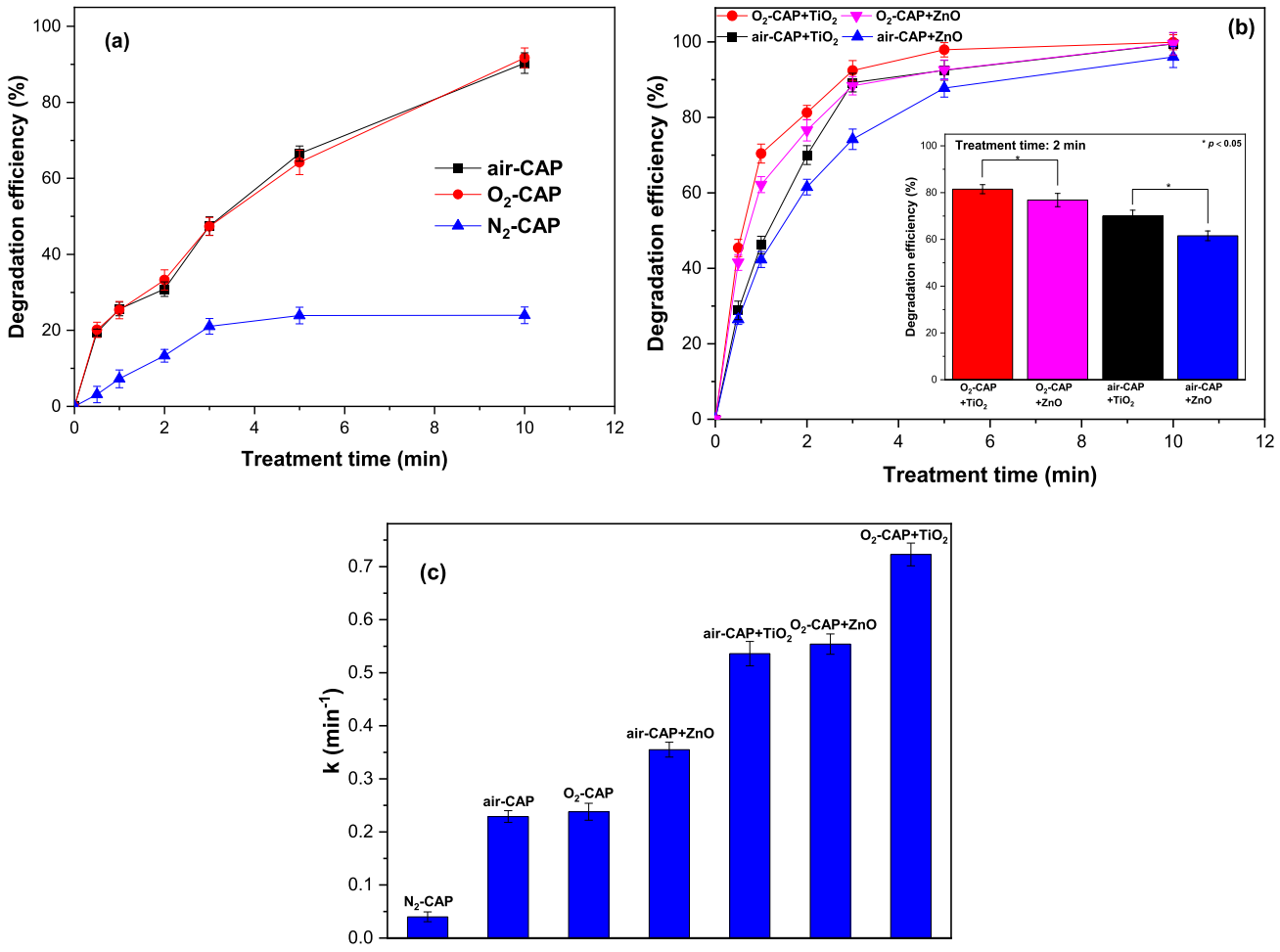

Fig. 4. (a) Trifluralin's degradation efficiency under air, oxygen and nitrogen atmosphere for plasma-alone process. (b) Effect of TiO_2 and ZnO on trifluralin's degradation efficiency under air and oxygen plasma (catalyst loading: 1 wt%) and (c) apparent rate constants under the various gases in the presence and absence of catalysts. Asterisk (*) indicates statistically significant differences ($p < 0.05$).

$$NO + O_3 \rightarrow NO_2 + O_2 \quad (10)$$

In addition, the limited trifluralin degradation under nitrogen gas indicated a limited role of the electrons and other RNS (reactions 11–12) generated during N_2-plasma in the degradation process.

$$N_2 + e^- \rightarrow e^- + 2N \quad (11)$$

$$N_2 + e^- \rightarrow N_2^+ + e^- \quad (12)$$

The comparison between O_2 and air plasma in the presence of TiO_2 and ZnO (1 wt%) is presented in Fig. 4b. In contrast to catalyst-free processes, a higher degradation rate was achieved with O_2 compared to air, indicative of increased ROS concentration when O_2 is used as the carrier gas. For example, after a 2 min treatment, degradation efficiency of trifluralin for 1 wt% TiO_2 was 78.3% and 70% when O_2 and air were used, respectively, while the corresponding values for 1 wt% ZnO were 76.6% and 61.5%. For both gases, at 2 min treatment, the addition of TiO_2 statistically significantly ($p < 0.05$) enhanced the degradation of trifluralin compared to ZnO. Nevertheless, at the end of the plasma treatment (i.e. 10 min), trifluralin was almost completely degraded under both O_2 and air in the presence of catalysts. In particular, the degradation efficiency was equal to 99.9% (O_2-CAP+TiO_2), 99.5% (O_2-CAP+ZnO), 99.4% (air-CAP+TiO_2) and 96% (air-CAP+ZnO). All data fitted a pseudo-first-order kinetic model (Fig. S5) with the apparent rate constant k being 0.72 (O_2-CAP+TiO_2) > 0.56 (O_2-CAP+ZnO) > 0.54 (air-CAP+TiO_2) and 0.36 min^{-1} (air-CAP+ZnO) (Fig. 4c). The higher pollutant degradation efficiency and rate achieved in the O_2-plasma+catalyst system might be due to the higher degree of O_3 decomposition to other ROS under O_2-plasma compared to air-plasma (see discussion in section 3.5). It is also possible that the very high energy photons (UVC radiation) emitted by O_2-plasma [56] resulted in more effective photo-activation of the catalyst compared to the UVA/UVB radiation in the case of air-plasma [57].

3.4. Effect of soil moisture on degradation efficiency in the absence and presence of catalysts

Another generally critical parameter proved to affect the degradation efficiency is the soil humidity. Soil moisture is affected by several factors including soil characteristics (soil texture, soil depth, physical structure and soil pores), organic matter, climate, etc., and therefore varies significantly, especially within the first meters below the surface. The water content may vary from 3% to 10% in sandy soil or from 20% to 40% in clay soil [58]. For this reason, we examined the effect of soil moisture up to 5% in the absence and presence of TiO_2 and ZnO, at representative soil moisture for sandy soils as the one under study. In

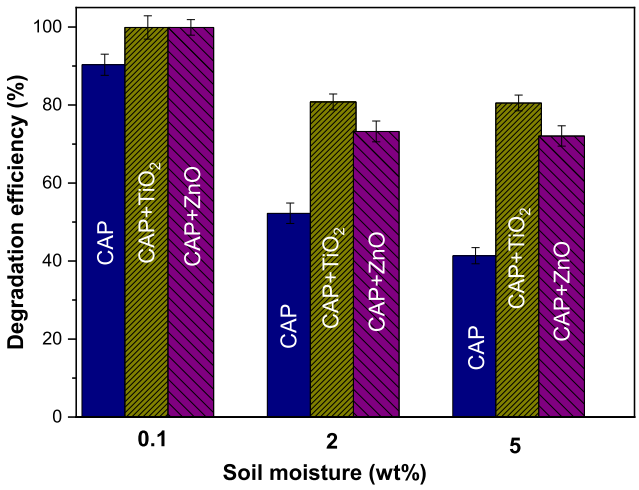

Fig. 5. Effect of soil moisture on trifluralin degradation efficiency in the presence and absence of TiO_2 and ZnO (plasma gas: air, catalyst loading: 2 wt%, treatment time: 10 min).

Fig. 5, the degradation efficiency is presented as a function of soil moisture. Obviously, the existence of water in soil seemed to decrease significantly the degradation efficiency of trifluralin during the air-plasma alone process. After a 10 min treatment, the removal of trifluralin in low moisture soil (~0.1 wt%) was 90.3%, whereas when soil moisture was 2 and 5 wt% it was reduced to 52.3 and 41.4%, respectively corresponding to a reduction of ~42% and ~54%. It has been already reported that the presence of soil moisture hinders the transport of plasma RONS in the soil bulk and their penetration in water prohibiting RONS/pollutant interactions, thus resulting in significant reduction of the pollutant degradation efficiency [6,16]. Nevertheless, as depicted in Fig. 5, the decrease of pollutant degradation in the presence of TiO_2 and ZnO was much lower compared to plasma alone and the impact of soil humidity becomes much less intense. For instance, during TiO_2-plasmacatalysis, trifluralin degradation efficiency decreased from 99.9% (0.1 wt% soil moisture) to 80.8 (2 wt% soil moisture) and 80.5% (5 wt% soil moisture) leading to a degradation reduction ~19% which is much lower compared to the ~54% degradation reduction observed for 5 wt% soil moisture during the plasma process without catalyst. This could be attributed to the fact that the presence of water molecules is considered a key-factor in the formation of active species on the surface of TiO_2 and ZnO during plasma [59,60]. The established reactions water molecules can be involved in the presence of appropriate catalysts to promote the generation of "new aqueous" active species are described in the following reactions:

$$TiO_2/ZnO + plasma \rightarrow e^- + h^+ \quad (13)$$

$$h^+ + H_2O \rightarrow {}^{\bullet}OH + H^+ \quad (14)$$

$$e^- + H_2O \rightarrow e^- + {}^{\bullet}H + {}^{\bullet}OH \quad (15)$$

$$O(^1D) + H_2O \rightarrow 2\ {}^{\bullet}OH \quad (16)$$

Therefore, the inhibitory effect of water molecules in preventing the plasma species to travel large distances through the soil pores and reach the pollutant, is partially offset by the ability of the catalysts to generate ROS locally that have to travel shorter distances to reach the pollutant. The plasma-catalytic mechanisms resulting in improved degradation performance are discussed in detail below.

3.5. Plasma species identification and quantification in the presence and absence of catalysts

3.5.1. OES measurements

For the identification of the main RONS we conducted OES measurements both in the absence and presence of the catalysts under air atmosphere (TiO_2 and ZnO); a representative emission spectrum for each case is illustrated in Fig. 1d. Similar excitation peaks were observed between the various plasma systems, nevertheless they varied in their intensity. The predominant detected species include the excited nitrogen molecules (N_2, Second Positive System) from 315 to 405 nm and the excited N_2^+ (First Negative System) from 390 to 440 nm caused by the electron-impact excitation and ionization of molecular nitrogen, respectively along with emissions for the ˙OH from 297 nm to 311 nm [61,62]. The weak emissions of O_2^+ at 427 and 527 nm [63], ˙O at 777 and 844 nm, Hγ at 434 nm and NOγ (230–280 nm) were also included [64,65]. The addition of TiO_2 and ZnO resulted in an alteration in the relative concentrations between RNS/ROS implying an enhancement of ROS concentrations in plasma+ZnO and plasma+TiO_2 systems compared to plasma alone. Therefore, ROS (e.g. ˙OH) is expected to have a significant role in the plasma-catalytic system for trifluralin degradation in soil. The ROS enhancement in the presence of catalysts is further supported by the exhaust gas analysis that follows.

3.5.2. O_3 and NO_x concentration in the plasma exhaust gases

Plasma-catalytic efforts for soil remediation are still very limited whereas the understanding of mechanisms involved remains challenging. O_3 and NO_x are among the main long-lived gaseous species produced during plasma. In order to move a step forward towards the understanding of the plasma-catalytic mechanism and the enhancement of the organic pollutant degradation efficiency (as already discussed in detail), O_3 and NO_x (NO and NO_2) concentrations were measured in the plasma exhaust gases in the presence and absence of TiO_2 and ZnO catalysts under both air and oxygen atmospheres (Fig. 6).

NO was not detected possibly due to its rapid overoxidation to NO_2 thus NO_x concentration is effectively equal to that of NO_2. This in turn implies that NO is destroyed fast and cannot have a major role in the degradation of trifluralin. The presence of TiO_2 and ZnO resulted in a significant increase in NO_2 concentration compared to the plasma alone process (Fig. 6); evidence of higher concentration of oxidizing species in the presence of catalysts. In particular, NO_2 concentration increased from 650 ppm (air-CAP) to 880 and 1168 at 1 wt% ZnO and 1 wt% TiO_2, respectively (Fig. 6a). On the other hand, when the percentage of the catalyst was increased to 2 wt%, the impact of the two catalysts was similar both on trifluralin degradation (Fig. 3c) and NO_2 concentration (Fig. 6b); NO_2 concentration was measured to be 1200 ppm and 1180 ppm for 2 wt% ZnO and 2 wt% TiO_2, respectively. This may be indicative of (i) reaching the concentration limit of certain plasma species in the presence of TiO_2 and (ii) involvement of NO_2 in the degradation of trifluralin.

The concentration of O_3 in the plasma alone was higher than that in the plasma+TiO_2 and plasma+ZnO systems both under air (Fig. 6c) and oxygen (Fig. 6d) atmospheres. In addition, in all cases the O_3 concentration was gradually increased with treatment time reaching a plateau after 2 or 3 min of treatment time. For air-plasma, the final O_3 concentration was ~1300 ppm and decreased to 750 ppm and 950 ppm in the presence of TiO_2 and ZnO, respectively (Fig. 6c). Under oxygen plasma, a much higher final O_3 concentration was measured (7000 ppm) which also significantly decreased to ~4000 ppm in the presence of TiO_2 or ZnO (Fig. 6d). The attenuation of O_3 concentration under catalytic conditions could be attributed to its catalyst-induced decomposition into other species [66,67], some of which at least, are probably actively involved in the degradation of trifluralin.

In particular, when plasma high-energy electrons and/or UV radiation activate the photocatalysts, holes and electrons are generated, while the photogenerated electrons can react with O_3 and reduce it to ozone

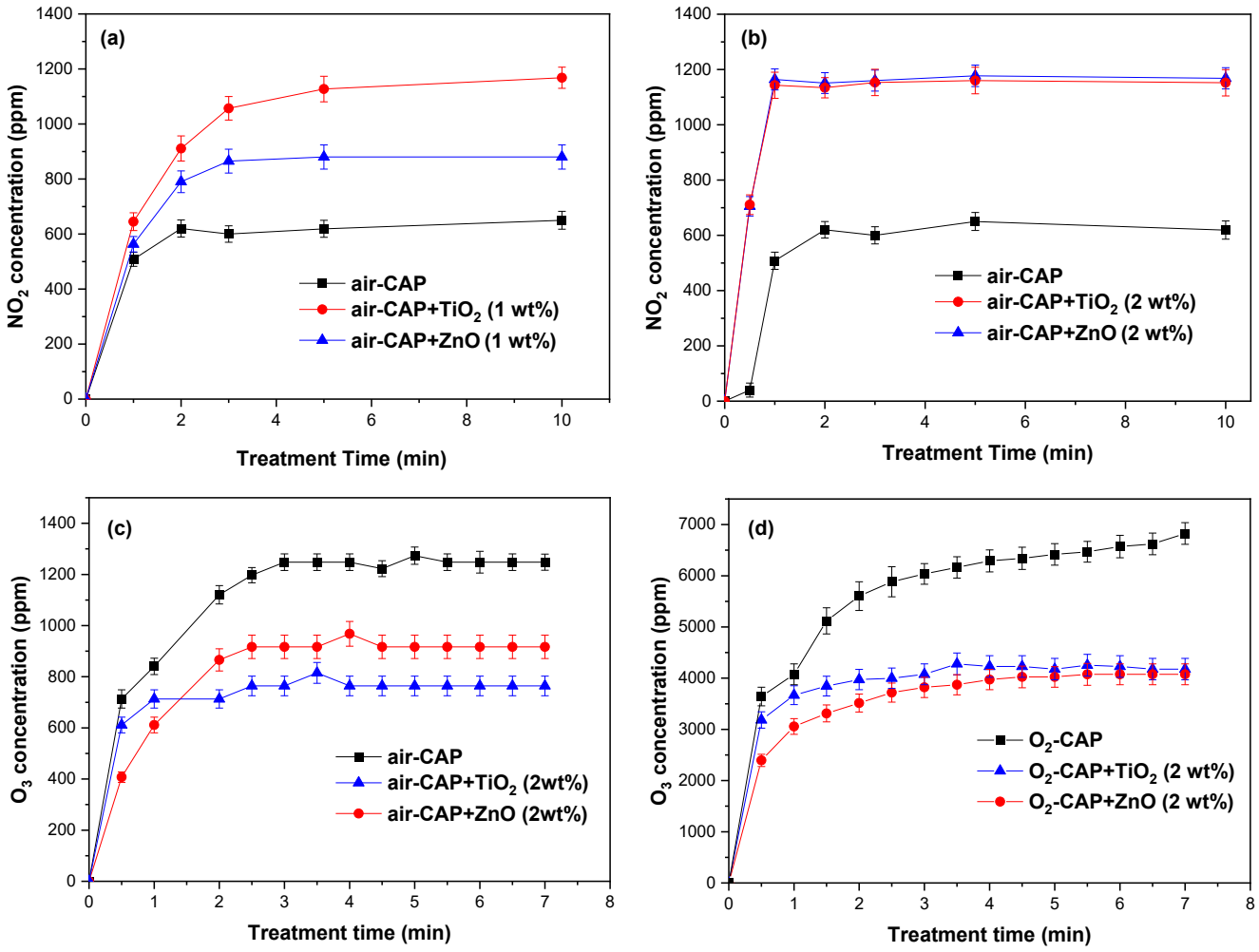

Fig. 6. Concentration of the plasma-generated NO_2 in the exhaust gases in the absence and presence of (a) 1 wt% and (b) 2 wt% of catalyst (plasma gas: air). Concentration of the plasma-generated O_3 in the exhaust gases in the absence and presence of catalyst during (c) air-plasma and (d) O_2-plasma (catalyst loading: 2 wt%).

radical (O_3^-) a highly active reactant (reaction (18) which recombines with O_3 to form O_4^- (reaction (19). This sequence of reactions may more than account for the decreased levels of O_3 in the presence of photocatalysts. Both O_3^- and O_4^- are short-lived species decomposing to produce O_2 (possibly in the singlet state too) and superoxide anions (O_2^-) through the reactions (20) and (21) [68] which enhance further the degradation of trifluralin. Additionally, O_3 can be decomposed on the catalyst surface resulting in the generation of atomic oxygen (reaction (22). Furthermore, additional superoxide anions can be generated through the reaction of e_{cb}^- and molecular oxygen (23) and the highly reactive OH radical resulting from h_{vb}^+ reacting with water present in the soil (reaction (24) [69]:

$$TiO_2/ZnO + plasma \rightarrow e_{cb}^- + h_{vb}^+ \quad (17)$$

$$O_3 + e_{cb}^- \rightarrow O_3^- \quad (18)$$

$$O_3^- + O_3 \rightarrow O_2 + O_4^- \quad (19)$$

$$2\ O_3^- \rightarrow O_2 + 2\ {}^{\bullet}O_2^- \quad (20)$$

$$O_4^- \rightarrow O_2 + {}^{\bullet}O_2^- \quad (21)$$

$$O_3 + * \rightarrow O_2 + {}^{\bullet}O* \quad (22)$$

$$O_2 + e_{cb}^- \rightarrow {}^{\bullet}O_2^- \quad (23)$$

$$h_{vb}^+ + H_2O \rightarrow {}^{\bullet}OH + H^+ \quad (24)$$

3.6. Proposed degradation pathways in the presence and absence of catalysts

Trifluralin is among the most common hazardous and persistent soil pollutants therefore its degradants in soil have been studied in detail [70]. Golab et al. compiled the first comprehensive catalogue of 43 trifluralin degradants and assigned a number to each one from TR2 to TR44 (TR1 being trifluralin) for future reference [71]. This systematic designation was adopted by regulating authorities [72], other researchers in this field, including us, by reporting newly identified trifluralin degradants with a new TR number, with the count continuing from the last reported one. In our previous article on plasma-induced trifluralin degradation in soil samples, we identified several new degradants and applied the same numbering system with the count reaching TR56 [15]. In this work we tentatively identified several new trifluralin degradants generated under plasma in the presence and

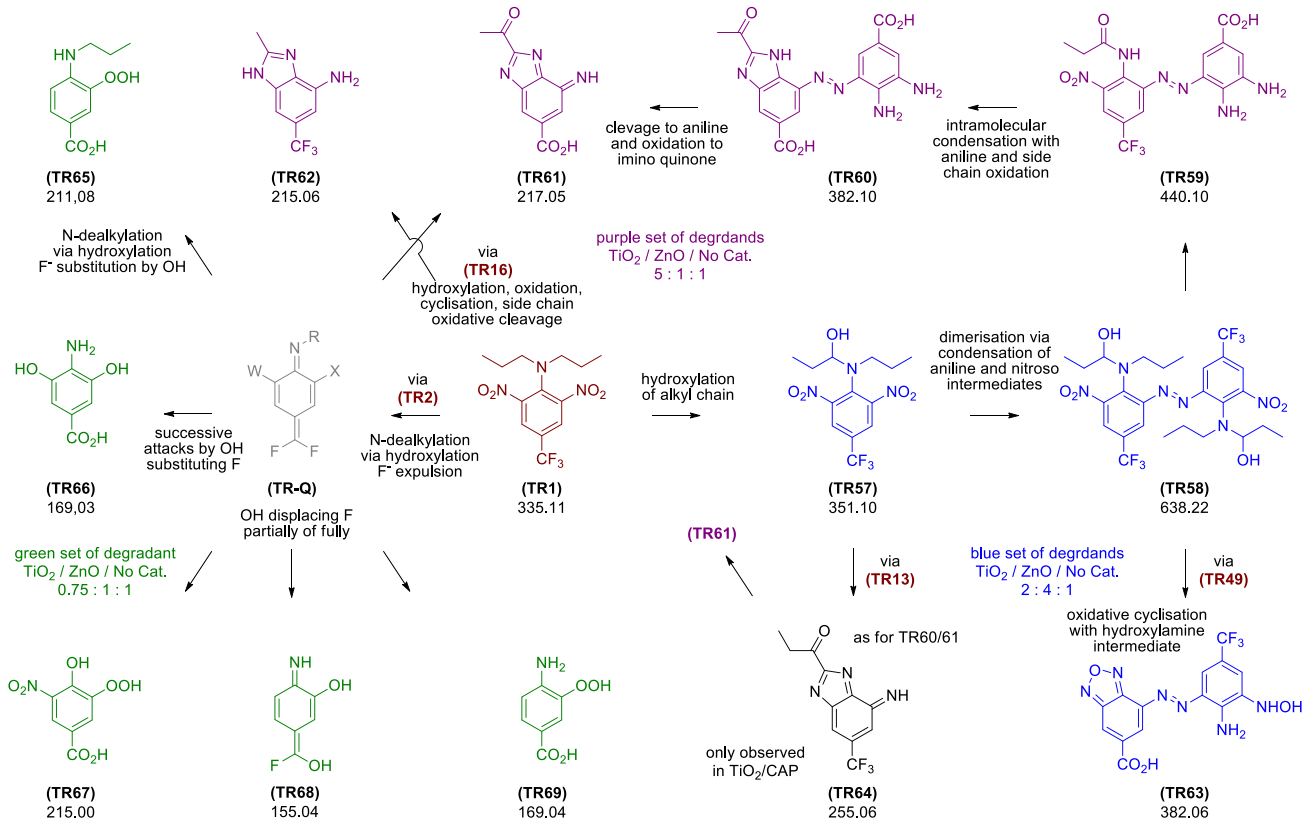

Fig. 7. Possible intermediate degradants and pathways involved in the plasma-induced degradation of trifluralin in soil with and without catalysts. The ratios indicated reflect the relative intensities of ionization in MS of the same set of species under the three different conditions (plasma gas: air, catalyst loading: 2 wt%, treatment time: 1 min).

absence of photocatalysts such as TiO_2 and ZnO. Following the established convention describe above, these were designated TR57-69 (Fig. 7).

In general, the trifluralin degradants found are consistent with those reported previously and the process appears to be governed by the same established reactions taking place under air/O_2-plasma conditions [15]. For example, the initial degradant of trifluralin is associated with hydroxylation of the alkyl chains at the carbon atom next to the nitrogen atom (TR57, Fig. 7) and the resulting hemiaminal may be hydrolyzed leading to dealkylated derivatives (essentially all TRs). The nitro groups are reduced by electron transfers successively to nitroso, hydroxylamine (TR63) and aniline intermediates (TR59, TR60) or may be replaced by OH/OOH (TR65, TR66, TR67, TR68 and TR69; green set of degradants), or may be cleaved entirely (TR65, TR68 and TR69). Hydroxylamine intermediate from partial reduction of nitro groups may participate in oxidative cyclizations giving rise to benzoxadiazoles such as the one in TR63. Finally, hemiaminal intermediates such as TR57 may be oxidized further to produce an amide (TR59) which may intramolecularly condense with an adjacent aniline to produce 2-alkylbenzimidazoles who may in turn suffer α-hydroxylation followed by further oxidation or ketones (TR60, TR61 and TR64) or fragmentation (TR62).

An interesting observation from this study is the fate of the trifluoromethyl group (CF3) present in trifluralin. In our previous work where we studied intermediate/late degradants we highlighted the survival of this group in the relatively high molecular products detected except in one that was found to have been converted to a carboxylic acid. In this study where early degradants were interrogated, we found that the CF3 group had been converted to carboxylic acid degradants in nearly half of the low molecular weight trifluralin degradants detected. This suggests that the CF3 conversion to carboxylic acids is more favorable in the early, trifluralin-like structures (degraded further and escaping detection at longer treatment times) while it becomes more resistant in the higher heterocycles and larger molecular weight species formed as degradation proceeds. Degradant TR68 is particularly important as it constitutes a signature of mechanism by which the CF3 group is metabolized. It appears that after partial or complete dealkylation of trifluralin and replacement/modification of at least one of the nitro groups into a less sterically demanding moiety, the resulting aniline can conjugate its electrons into the *para*-position of the aromatic ring and expel a fluoride anion from the CF3 group giving rise to a benzoquinone imine type of intermediate (TR-Q, R = H or propyl). This is not possible in the parent trifluralin as the N-substituents at the sp2 hybridized nitrogen would clash with the large nitro groups. Successive hydroxyl attacks at the difuoroalkenyl carbon atom of TR-Q type of intermediates lead to the formation of carboxylic acid. The high reactivity of TR-Qs is undoubtedly responsible for escaping detection (hence grey and no number assigned in Fig. 7), yet they are the most probable and reasonable precursors to TR68 and the members of the green set of carboxylic acid degradants. It is also possible that the carboxylic acid groups found in some of the dimeric degradants, is formed in this way prior to a dimerization process (TR61 precursor to TR60) although hydrolysis of the CF3 group post dimerization may equally happen via related quinoid intermediates. The increased degradation of CF3 is prime importance as this group, aside from its electron-withdrawing and lipophilic properties, is frequently installed in drug molecules and agrochemicals to impart metabolic/oxidative stability and survive long enough to exert their biological effects. On the other hand, this undermines the natural and non-natural degradation of fluorinated molecules. The present work supports an important development in degrading efficiently metabolically resistant fluorinated molecules such as PFAS, that constitute a challenge in modern remediation technologies.

In terms of similarities and differences among the plasma+TiO_2, plasma+ZnO and plasma alone processes it appears that the TR-Q

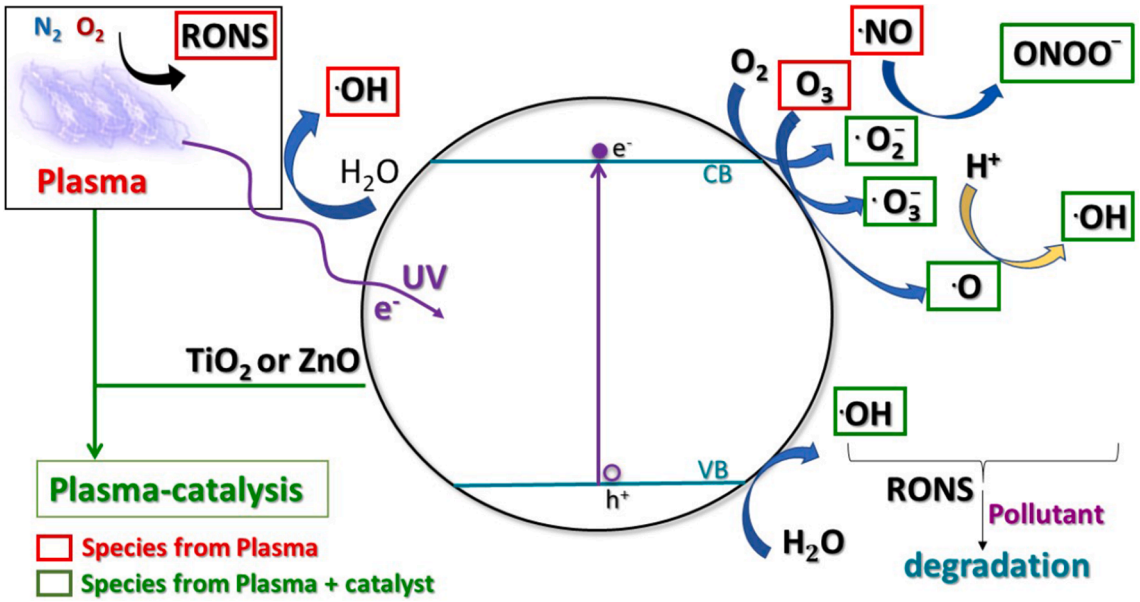

Fig. 8. A schematic representation of possible plasma-catalytic processes related to pollutant degradation.

pathway (green set of degradants, Fig. 7) is favored the most under all conditions and the degradants resulting from this pathway are the most abundant. Nevertheless, the plasma alone process and that containing ZnO (plasma+ZnO) are more similar to one another whereas the plasma+TiO_2 process differs slightly in terms of preferred degradation pathways. Finally, the catalysts besides their limited contact with the solid pollutant, it is possible that they participate in a photocatalytic reaction pathway that involves electron transfers to and from the pollutant generating pollutant species with increased reactivity.

Conclusively, based on the findings already presented herein related to (i) catalysts characterization after plasma treatment, (ii) differences in the concentration of RONS between plasma alone and plasma-catalysis, (iii) enhancement of pollutant degradation efficiency/rate/energy efficiency in the presence of TiO_2/ZnO catalysts under the various conditions (catalyst type/loading, plasma gas, soil humidity, etc.) and (iv) plasma-induced intermediates of pollutant degradation in the presence and absence of catalysts, a possible plasma-catalytic mechanism for the degradation of organic pollutants in soil is presented in Fig. 8.

4. Conclusions

A plasma reactor driven by HV nanopulses and capable of producing micro-discharges directly into the interconnected soil channels was combined with TiO_2 and ZnO catalysts for the degradation of trifluralin. The presence of both catalysts enhanced substantially the degradation efficiency/rate resulting in complete and high energy-efficient pollutant degradation. The energy efficiency of the plasma-catalytic process increased 3-fold compared to plasma alone with a maximum of ~22 mg of pollutant/kJ and ~410 kg of soil/kWh. In the presence of TiO_2 and ZnO a significant increase in NO_2 concentration and a noticeable reduction of O_3 was recorded with the latter being converted to more active ROS. For both catalysts, O_2-plasma revealed a better performance compared to air-plasma, attributed to additional O_3 decomposition and ROS enhancement and/or higher energy of photons when O_2 was used as the plasma carrier gas. The order in pollutant degradation kinetics was O_2-plasma+TiO_2 > O_2-plasma+ZnO > air-plasma+TiO_2 > air-plasma+ZnO > O_2-plasma ≈ air-plasma. The previously known inhibitory effect of the soil humidity on pollutant degradation was less intense in the presence of catalysts; i.e. the reduction in trifluralin degradation was ~19% in the presence of TiO_2, much lower than the ~54% reduction during the plasma-alone process. The degradation pathways were elucidated revealing similar processes between plasma-alone and plasma-catalysis. Furthermore, a significant number of trifluralin degradants detected in this study have the parent trifluoromethyl group converted to carboxylic acid. This increased degradation of fluorinated groups is particularly encouraging and holds promise in developing our process further to encompass degradation of polyfluorinated pollutants such as PFAS. Overall, this study provides useful insights on the plasma-catalytic mechanisms towards a highly-efficient and sustainable soil remediation approach.

CRediT authorship contribution statement

M. Hatzisymeon: Investigation, Visualization. **M.K. Daletou:** Methodology, Investigation, Writing – review & editing. **G. Rassias:** Methodology, Investigation, Writing – review & editing. **C.A. Aggelopoulos:** Conceptualization, Methodology, Investigation, Visualization, Supervision, Resources, Writing – original draft, Writing – review & editing, Funding acquisition.

Declaration of Competing Interest

The authors declare that they have no known competing financial interests or personal relationships that could have appeared to influence the work reported in this paper.

Data availability

Data will be made available on request.

Acknowledgements

This project has received funding from the European Union's Horizon 2020 research and innovation programme under grant agreement No101037509. TEM measurements were performed at the Electron Microscopy and Microanalysis Laboratory, University of Patras.

Appendix A. Supplementary data

Supplementary data to this article can be found online at https://doi.org/10.1016/j.seppur.2023.124119.

References

[1] J.M. Tor, C. Xu, J.M. Stucki, M.M. Wander, G.K. Sims, Trifluralin Degradation under Microbiologically Induced Nitrate and Fe(III) Reducing Conditions, Environ. Sci. Tech. 34 (2000) 3148–3152.

[2] C.A. Aggelopoulos, Recent advances of cold plasma technology for water and soil remediation: A critical review, Chem. Eng. J. 428 (2022), 131657.

[3] C.A. Aggelopoulos, Atmospheric pressure dielectric barrier discharge for the remediation of soil contaminated by organic pollutants, Int. J. Environ. Sci. Technol. 13 (2016) 1731–1740.

[4] H. Zhang, D. Ma, R. Qiu, Y. Tang, C. Du, Non-thermal plasma technology for organic contaminated soil remediation: A review, Chem. Eng. J. 313 (2017) 157–170.

[5] H. Guo, Y. Wang, L. Liao, Z. Li, S. Pan, C. Puyang, Y. Su, Y. Zhang, T. Wang, J. Ren, J. Li, Review on remediation of organic-contaminated soil by discharge plasma: Plasma types, impact factors, plasma-assisted catalysis, and indexes for remediation, Chem. Eng. J. 436 (2022), 135239.

[6] J. Zhao, A. Zhang, P. Héroux, Z. Sun, Y. Liu, Remediation of diesel fuel polluted soil using dielectric barrier discharge plasma, Chem. Eng. J. 417 (2021), 128143.

[7] C.A. Aggelopoulos, A. Gkelios, M.I. Klapa, C. Kaltsonoudis, P. Svarnas, C. D. Tsakiroglou, Parametric analysis of the operation of a non-thermal plasma reactor for the remediation of NAPL-polluted soils, Chem. Eng. J. 301 (2016) 353–361.

[8] C.A. Aggelopoulos, P. Svarnas, M.I. Klapa, C.D. Tsakiroglou, Dielectric barrier discharge plasma used as a means for the remediation of soils contaminated by non-aqueous phase liquids, Chem. Eng. J. 270 (2015) 428–436.

[9] J. Zhan, Y. Liu, W. Cheng, A. Zhang, R. Li, X. Li, S. Ognier, S. Cai, C. Yang, J. Liu, Remediation of soil contaminated by fluorene using needle-plate pulsed corona discharge plasma, Chem. Eng. J. 334 (2018) 2124–2133.

[10] Y. Abbas, W. Lu, Q. Wang, H. Dai, Y. Liu, X. Fu, C. Pan, H. Ghaedi, F. Cheng, H. Wang, Remediation of pyrene contaminated soil by double dielectric barrier discharge plasma technology: Performance optimization and evaluation, Environ. Pollut. 260 (2020), 113944.

[11] T. Wang, J. Ren, G. Qu, D. Liang, S. Hu, Glyphosate contaminated soil remediation by atmospheric pressure dielectric barrier discharge plasma and its residual toxicity evaluation, J. Hazard. Mater. 320 (2016) 539–546.

[12] C.A. Aggelopoulos, D. Tataraki, G. Rassias, Degradation of atrazine in soil by dielectric barrier discharge plasma – Potential singlet oxygen mediation, Chem. Eng. J. 347 (2018) 682–694.

[13] J. Zhan, A. Zhang, P. Héroux, Y. Guo, Z. Sun, Z. Li, J. Zhao, Y. Liu, Remediation of perfluorooctanoic acid (PFOA) polluted soil using pulsed corona discharge plasma, J. Hazard. Mater. 387 (2020), 121688.

[14] C.A. Aggelopoulos, C.D. Tsakiroglou, A new perspective towards in-situ cold plasma remediation of polluted sites: Direct generation of micro-discharges within contaminated medium, Chemosphere 266 (2021), 128969.

[15] M. Hatzisymeon, D. Tataraki, G. Rassias, C.A. Aggelopoulos, Novel combination of high voltage nanopulses and in-soil generated plasma micro-discharges applied for the highly efficient degradation of trifluralin, J. Hazard. Mater. 415 (2021), 125646.

[16] M. Hatzisymeon, D. Tataraki, C. Tsakiroglou, G. Rassias, C.A. Aggelopoulos, Highly energy-efficient degradation of antibiotics in soil: Extensive cold plasma discharges generation in soil pores driven by high voltage nanopulses, Sci. Total Environ. 786 (2021), 147420.

[17] S. Meropoulis, S. Giannoulia, S. Skandalis, G. Rassias, C.A. Aggelopoulos, Key-study on plasma-induced degradation of cephalosporins in water: Process optimization, assessment of degradation mechanisms and residual toxicity, Sep. Purif. Technol. 298 (2022), 121639.

[18] M. Russo, G. Iervolino, V. Vaiano, V. Palma, Non-Thermal Plasma Coupled with Catalyst for the Degradation of Water Pollutants: A Review, Catalysts 10 (2020) 1438.

[19] N. Korichi, O. Aubry, H. Rabat, B. Cagnon, D. Hong, Paracetamol Degradation by Catalyst Enhanced Non-Thermal Plasma Process for a Drastic Increase in the Mineralization Rate, Catalysts 10 (2020) 959.

[20] J. Fan, H. Wu, R. Liu, L. Meng, Y. Sun, Review on the treatment of organic wastewater by discharge plasma combined with oxidants and catalysts, Environ. Sci. Pollut. Res. 28 (2021) 2522–2548.

[21] T.C. Wang, N. Lu, J. Li, Y. Wu, Plasma-TiO_2 Catalytic Method for High-Efficiency Remediation of p-Nitrophenol Contaminated Soil in Pulsed Discharge, Environ. Sci. Tech. 45 (2011) 9301–9307.

[22] T. Wang, N. Lu, J. Li, Y. Wu, Y. Su, Enhanced degradation of p-nitrophenol in soil in a pulsed discharge plasma-catalytic system, J. Hazard. Mater. 195 (2011) 276–280.

[23] Y. Liu, J. Liang, X. Zhou, H. Yuan, Y. Li, D. Chang, K. Yang, D. Yang, Degradation of persistent organic pollutants in soil by parallel tubes-array dielectric barrier discharge plasma cooperating with catalyst, Chem. Eng. J. 437 (2022), 135089.

[24] H. Lu, C. Deng, Z. Yu, D. Zhang, W. Li, J. Huang, T. Bao, X. Liu, Synergistic degradation of fluorene in soil by dielectric barrier discharge plasma combined with P25/NH2-MIL-125(Ti), Chemosphere 296 (2022), 133950.

[25] J. Lou, N. Lu, J. Li, T. Wang, Y. Wu, Remediation of chloramphenicol-contaminated soil by atmospheric pressure dielectric barrier discharge, Chem. Eng. J. 180 (2012) 99–105.

[26] N. Lu, C. Wang, C. Lou, J. Li, K. Shang, Y. Wu, Combination of pulsed corona discharge plasma and gamma-Al_2O_3-supported catalysts for polycyclic aromatic hydrocarbon removal in soil, Sep. Purif. Technol. 156 (2015) 766–771.

[27] S. Hernández, D. Hidalgo, A. Sacco, A. Chiodoni, A. Lamberti, V. Cauda, E. Tresso, G. Saracco, Comparison of photocatalytic and transport properties of TiO_2 and ZnO nanostructures for solar-driven water splitting, PCCP 17 (2015) 7775–7786.

[28] D. Chen, Y. Cheng, N. Zhou, P. Chen, Y. Wang, K. Li, S. Huo, P. Cheng, P. Peng, R. Zhang, L. Wang, H. Liu, Y. Liu, R. Ruan, Photocatalytic degradation of organic pollutants using TiO_2-based photocatalysts: A review, J. Clean. Prod. 268 (2020), 121725.

[29] M.R. Al-Mamun, S. Kader, M.S. Islam, M.Z.H. Khan, Photocatalytic activity improvement and application of UV-TiO_2 photocatalysis in textile wastewater treatment: A review, J. Environ. Chem. Eng. 7 (2019), 103248.

[30] S.H. Khan, B. Pathak, Zinc oxide based photocatalytic degradation of persistent pesticides: A comprehensive review, Environ. Nanotechnol. Monit. Manage. 13 (2020), 100290.

[31] K.M. Lee, C.W. Lai, K.S. Ngai, J.C. Juan, Recent developments of zinc oxide based photocatalyst in water treatment technology: A review, Water Res. 88 (2016) 428–448.

[32] I.F. Chowdhury, M. Rohan, B.J. Stodart, C. Chen, H. Wu, G.S. Doran, Persistence of atrazine and trifluralin in a clay loam soil undergoing different temperature and moisture conditions, Environ. Pollut. 276 (2021), 116687.

[33] T.C. Wang, G. Qu, J. Li, D. Liang, S. Hu, Depth dependence of p-nitrophenol removal in soil by pulsed discharge plasma, Chem. Eng. J. 239 (2014) 178–184.

[34] C.A. Aggelopoulos, M. Hatzisymeon, D. Tataraki, G. Rassias, Remediation of ciprofloxacin-contaminated soil by nanosecond pulsed dielectric barrier discharge plasma: Influencing factors and degradation mechanisms, Chem. Eng. J. 393 (2020), 124768.

[35] W. Xie, R. Li, Q. Xu, Enhanced photocatalytic activity of Se-doped TiO2 under visible light irradiation, Sci. Rep. 8 (2018) 8752.

[36] B. Bharti, S. Kumar, H.-N. Lee, R. Kumar, Formation of oxygen vacancies and Ti3+ state in TiO2 thin film and enhanced optical properties by air plasma treatment, Sci. Rep. 6 (2016) 32355.

[37] C.-Y. Tsai, H.-C. Hsi, T.-H. Kuo, Y.-M. Chang, J.-H. Liou, Preparation of Cu-Doped TiO_2 Photocatalyst with Thermal Plasma Torch for Low-Concentration Mercury Removal, Aerosol Air Qual. Res. 13 (2013) 639–648.

[38] A.K. Zak, R. Razali, W.H. Majid, M. Darroudi, Synthesis and characterization of a narrow size distribution of zinc oxide nanoparticles, Int. J. Nanomed. 6 (2011) 1399–1403.

[39] G. Panchal, D.K. Shukla, R.J. Choudhary, V.R. Reddy, D.M. Phase, The effect of oxygen stoichiometry at the interface of epitaxial $BaTiO_3/La_{0.7}Sr_{0.3}MnO_3$ bilayers on its electronic and magnetic properties, J. Appl. Phys. 122 (2017), 085310.

[40] T. Zhang, S. Cui, B. Yu, Z. Liu, D. Wang, Surface engineering for an enhanced photoelectrochemical response of TiO_2 nanotube arrays by simple surface air plasma treatment, Chem. Commun. 51 (2015) 16940–16943.

[41] A.K. Rumaiz, B. Ali, A. Ceylan, M. Boggs, T. Beebe, S. Ismat Shah, Experimental studies on vacancy induced ferromagnetism in undoped TiO_2, Solid State Commun. 144 (2007) 334–338.

[42] R. Asahi, T. Morikawa, T. Ohwaki, K. Aoki, Y. Taga, Visible-Light Photocatalysis in Nitrogen-Doped Titanium Oxides, Science 293 (2001) 269–271.

[43] M. Claros, M. Setka, Y.P. Jimenez, S. Vallejos, AACVD Synthesis and Characterization of Iron and Copper Oxides Modified ZnO Structured Films, in: Nanomaterials, 2020.

[44] R. Ahmad, N. Tripathy, M.Y. Khan, K.S. Bhat, M.-S. Ahn, Y.-B. Hahn, Ammonium ion detection in solution using vertically grown ZnO nanorod based field-effect transistor, RSC Adv. 6 (2016) 54836–54840.

[45] N.G. A. Sahai, Solid State Physics AIP Conf. Proc. 050023-1–050023-3, 1665.

[46] Y. Sun, J.H. Seo, C.J. Takacs, J. Seifter, A.J. Heeger, Inverted Polymer Solar Cells Integrated with a Low-Temperature-Annealed Sol-Gel-Derived ZnO Film as an Electron Transport Layer, Adv. Mater. 23 (2011) 1679–1683.

[47] M.-C. Chu, J.S. Meena, P.-T. Liu, H.-P.-D. Shieh, H.-C. You, Y.-W. Tu, F.-C. Chang, F.-H. Ko, Oxygen Plasma Functioning of Charge Carrier Density in Zinc Oxide Thin-Film Transistors, Appl. Phys Express 6 (2013), 076501.

[48] U. Ilyas, R.S. Rawat, T.L. Tan, P. Lee, R. Chen, H.D. Sun, L. Fengji, S. Zhang, Oxygen rich p-type ZnO thin films using wet chemical route with enhanced carrier concentration by temperature-dependent tuning of acceptor defects, J. Appl. Phys. 110 (2011), 093522.

[49] A.-A. Talukder, J. Pokharel, M. Shrestha, Q.H. Fan, Improving electrical properties of sol-gel derived zinc oxide thin films by plasma treatment, J. Appl. Phys. 120 (2016), 155303.

[50] H. Jiang, S. Liu, L. Liang, W. Lu, Oxygen plasma assisted enhanced photoresponse of ZnO nanowires fabricated by catalyst-free chemical vapor deposition, RSC Adv. 8 (2018) 28928–28933.

[51] N. Lu, C. Wang, C. Lou, Remediation of PAH-contaminated soil by pulsed corona discharge plasma, J. Soil. Sediment. 17 (2017) 97–105.

[52] H. Guo, Y. Wang, X. Yao, Y. Zhang, Z. Li, S. Pan, J. Han, L. Xu, W. Qiao, J. Li, H. Wang, A comprehensive insight into plasma-catalytic removal of antibiotic oxytetracycline based on graphene-TiO_2-Fe_3O_4 nanocomposites, Chem. Eng. J. 425 (2021), 130614.

[53] H. Guo, N. Jiang, H. Wang, N. Lu, K. Shang, J. Li, Y. Wu, Degradation of antibiotic chloramphenicol in water by pulsed discharge plasma combined with TiO_2/WO_3 composites: mechanism and degradation pathway, J. Hazard. Mater. 371 (2019) 666–676.

[54] M. Ansari, A. Hossein Mahvi, M. Hossein Salmani, M. Sharifian, H. Fallahzadeh, M. Hassan Ehrampoush, Dielectric barrier discharge plasma combined with nano catalyst for aqueous amoxicillin removal: Performance modeling, kinetics and optimization study, energy yield, degradation pathway, and toxicity, Sep. Purif. Technol. 251 (2020), 117270.

[55] J. Zhan, A. Zhang, P. Héroux, X. Li, Z. Li, J. Zhao, Y. Guo, Y. Liu, Gasoline degradation and nitrogen fixation in soil by pulsed corona discharge plasma, Sci. Total Environ. 661 (2019) 266–275.
[56] M. Jaritz, H. Behm, C. Hopmann, D. Kirchheim, F. Mitschker, P. Awakowicz, R. Dahlmann, The effect of UV radiation from oxygen and argon plasma on the adhesion of organosilicon coatings on polypropylene, J. Phys. D Appl. Phys. 50 (2017), 015201.
[57] P. Thana, A. Wijaikhum, P. Poramapijitwat, C. Kuensaen, J. Meerak, A. Ngamjarurojana, S. Sarapirom, D. Boonyawan, A compact pulse-modulation cold air plasma jet for the inactivation of chronic wound bacteria: development and characterization, Heliyon 5 (2019) e02455.
[58] M.J. Brandt, K.M. Johnson, A.J. Elphinston, D.D. Ratnayaka, Chapter 3 - Hydrology and Surface Supplies, in: M.J. Brandt, K.M. Johnson, A.J. Elphinston, D. D. Ratnayaka (Eds.), Twort's Water Supply (Seventh Edition), Butterworth-Heinemann, Boston, 2017, pp. 65–116.
[59] L. Duan, S. Rao, D. Wang, K. Zhang, H. Cao, Z. Liu, Q. Guo, W. Li, J. Tao, Y. Gao, Understanding of TiO2 catalysis mechanism in underwater pulsed discharge system: Charge carrier generation and interfacial charge-transfer processes, Chemosphere 267 (2021), 129249.
[60] X. Yan, C. Yi, Y. Wang, W. Cao, D. Mao, Q. Ou, P. Shen, H. Wang, Multi-catalysis of nano-zinc oxide for bisphenol A degradation in a dielectric barrier discharge plasma system: Effect and mechanism, Sep. Purif. Technol. 231 (2020), 115897.
[61] C.A. Aggelopoulos, S. Meropoulis, M. Hatzisymeon, Z.G. Lada, G. Rassias, Degradation of antibiotic enrofloxacin in water by gas-liquid nsp-DBD plasma: Parametric analysis, effect of H_2O_2 and CaO_2 additives and exploration of degradation mechanisms, Chem. Eng. J. 398 (2020), 125622.
[62] P. Jamróz, P. Pohl, W. Żyrnicki, Spectroscopic evaluation of a low power atmospheric pressure mixed argon–helium microwave induced plasma combined with the chemical generation of volatile species for the optical emission spectrometric determination of arsenic, antimony and mercury, J. Anal. At. Spectrom 27 (2012) 1772–1779.
[63] T. Chang, Z. Shen, Y. Huang, J. Lu, D. Ren, J. Sun, J. Cao, H. Liu, Post-plasma-catalytic removal of toluene using MnO_2–Co_3O_4 catalysts and their synergistic mechanism, Chem. Eng. J. 348 (2018) 15–25.
[64] J. Kim, B. Ghimire, S. Lim, E.H. Choi, H.-K. Park, N.K. Kaushik, Coagulation, deformability, and aggregation of RBCs and platelets following exposure to dielectric barrier discharge plasma with the use of different feeding gases, J. Phys. D Appl. Phys. 52 (2019), 155202.
[65] F. Rezaei, M. Abbasi-Firouzjah, B. Shokri, Investigation of antibacterial and wettability behaviours of plasma-modified PMMA films for application in ophthalmology, J. Phys. D Appl. Phys. 47 (2014), 085401.
[66] H. Song, F. Hu, Y. Peng, K. Li, S. Bai, J. Li, Non-thermal plasma catalysis for chlorobenzene removal over CoMn/TiO_2 and CeMn/TiO_2: Synergistic effect of chemical catalysis and dielectric constant, Chem. Eng. J. 347 (2018) 447–454.
[67] L. Jiang, G. Nie, R. Zhu, J. Wang, J. Chen, Y. Mao, Z. Cheng, W.A. Anderson, Efficient degradation of chlorobenzene in a non-thermal plasma catalytic reactor supported on CeO_2/HZSM-5 catalysts, J. Environ. Sci. 55 (2017) 266–273.
[68] J. Patzsch, J.Z. Bloh, Improved photocatalytic ozone abatement over transition metal-grafted titanium dioxide, Catal. Today 300 (2018) 2–11.
[69] L. Zhang, P. Li, Z. Gong, X. Li, Photocatalytic degradation of polycyclic aromatic hydrocarbons on soil surfaces using TiO_2 under UV light, J. Hazard. Mater. 158 (2008) 478–484.
[70] W. Sang, J. Cui, L. Mei, Q. Zhang, Y. Li, D. Li, W. Zhang, Z. Li, Degradation of liquid phase N, N-dimethylformamide by dielectric barrier discharge plasma: Mechanism and degradation pathways, Chemosphere 236 (2019), 124401.
[71] T. Golab, W.A. Althaus, H.L. Wooten, Fate of [14C]trifluralin in soil, J. Agric. Food Chem. 27 (1979) 163–179.
[72] R.N. Lerch, I. Ferrer, E.M. Thurman, R.M. Zablotowicz, Identification of Trifluralin Metabolites in Soil Using Ion-Trap LC/MS/MS, in: Liquid Chromatography/Mass Spectrometry, MS/MS and Time of Flight MS, American Chemical Society, 2003, pp. 291–310.